Sub Topic: Internal Combustion and Gas Turbine Engines

SAND2017-2157C

10th U. S. National Combustion Meeting
Organized by the Eastern States Section of the Combustion Institute
April 23-26, 2017
College Park, Maryland

Comparing infrared emission from hydrocarbon C-H stretch during direct injection with and without reaction in an optical heavy duty engine

W. Ethan Eagle[1a], Greg Roberts[2], Mark P.B. Musculus[2], Louis-Marie Malbec[3a], Luigi Sequino[4a], and Ezio Mancaruso[4a]*

[1]Mechanical Engineering, Wayne State University, Detroit MI, USA
[2]Engine Research Department, Combustion Research Facility, Livermore CA, USA
[3]IFPEN, Paris, France
[4]Istituto Motori, Naples, Italy
[a]Work completed at Sandia, CRF [*]Corresponding Author Email: ethaneagle@wayne.edu

Abstract: We present new imaging data comparing IR emission near 3.4 micron of non-reacting and reacting fuel jets from a 9:1 skip-fired optical engine. Images are shown for 3, 5, 7, and 10 crank-angle degrees after the start of injection at three top-dead-center ambient gas temperatures, 800 K 900 K and 1000 K. In addition to presenting qualitative instantaneous 2D images, we quantify differences using ensemble averaged longitudinal profiles of the non-reacting and reacting jets. We see that reaction increases emission by a factor of 2 to 3 during the jet development, prior to bowl-wall interaction. Following bowl-wall interaction, emission increases by a factor of more than 7. The influence of soot emission on the infrared signal is investigated with references to the 'Spray A' free jet from the Engine Combustion Network (ECN). The engine experimental in-cylinder condition is the ECN 900 K, 15.2 kg/m^3, 1500 bar rail-pressure injection with n-dodecane fuel. From prior ECN data, hot soot formed under similar conditions should emit 2 to 5 times more than unreacted vapor fuel. Improved diagnostics, e.g. simultaneous measurement of soot volume fraction with IR emission, are needed to provide insight about the fate and transport of unburned fuel in the presence of soot.
Keywords: Reacting Diesel Jets, Infrared Imaging, Optical Engines, Vapor Fuel Penetration

1. Introduction

Controlling fuel-air mixing both before and during combustion is critical to efficiency and pollutant emissions of diesel engines. Optical diagnostics for in-cylinder fuel-vapor tracking can be helpful to better understand how engines can be designed and operated to optimize mixing. For example, fuel-jet penetration and spreading are direct consequences of mixing, such that tracking in-cylinder vapor fuel provides information about mixing. Therefore, techniques that can identify in-cylinder vapor-jet penetration and spreading of fuel are of interest.

Relative to schlieren (and laser-based) imaging, IR emission imaging is attractive because it does not require an external light source or pass-through optical access, so it can be applied to more practical combustion devices with less optical access and at lower expense. Additionally, the transmission of UV-grade fused silica permits fuel vapor imaging by detecting C-H stretch-band thermal emission near 3.3-3.4 micron. The viability of infrared detection for this purpose has yet to be proven under reacting conditions.

Other previous work can help us to understand where to look and identifies the 3.3-3.4 micron band as attractive for fuel-vapor IR imaging [1–4]. Previous investigations with IR imaging of combustion assess H_2O and CO_2 formation at 2.4-2.5 micron [5] and CO at 3.9 micron [6,7]. The influence of soot was preliminarily assessed [8] using broad-band detection from 3 to 5 micron. However, reference data

for direct comparison of non-reacting with reacting cases for emission from hydrocarbons under different stages of combustion is not readily available.

In this paper, we aim to extend our IR emission-imaging technique filtered at 3.2-3.5 micron to compare how the signals can be interpreted under combusting conditions. Non-reacting conditions are compared to combusting conditions for three in-cylinder compressed-gas temperatures. This extends our previous work, which developed a simple non-reacting one-dimensional (1D) transient gas-jet model using a prescribed steady-jet radial fuel concentration profiles to estimate IR emission/absorption [9]. Also new here, we make use of measured soot data from the engine combustion network database for the 'Spray A' single jet condition, to make a conservative estimate for the ratio of soot emission to fuel-vapor emission.

2. Experimental Methods

The Sandia single-cylinder 2.34 L-displacement optical heavy-duty diesel engine is based on the Cummins N-series production line. The engine has optical access for IR imaging up through an extended piston and flat UV-grade fused-silica piston-crown window depicted in Fig. 1. Although fused silica is not broadly IR transparent, a narrow region near 3.4 micron is sufficiently transparent (>80%) for imaging C-H stretch-band emission from hydrocarbons. The fuel injector is from the Engine Combustion Network (ECN) family, 'Spray B,' #211199. The fuel is n-dodecane (>99.2% purity) delivered from Sigma Aldrich. To save space here, more detailed specifications on the engine and injector can be found in [10,11].

Infrared imaging of in-cylinder hydrocarbon fuel jets in which the vapor-phase fuel has been heated by mixing with compressed ambient gases primarily detects emission from the C-H stretch band centered near 3.4 micron. (Peak spectral content is between 3361-3448nm 2975-2900cm^{-1}[4]). From methane to n-hexadecane, the emission cross-section varies approximately linearly with the number of C-H bonds, with different dependencies for different bond type (paraffinic, aromatic, naphthalenic, etc.) [12].

The intensity of C-H stretch emission from non-reacting fuel jets depends on the optical path length, fuel concentration, and temperature. For round jets viewed from the side, the optical path length and path-length-averaged fuel concentration vary proportionally and approximately inverse-proportionally, respectively, with downstream distance [9]. For cold fuel jets injected into a hot ambient gas, the temperature increases along the jet axis. Hence, the variation along the jet axis of the first two effects compensate for each other, leaving

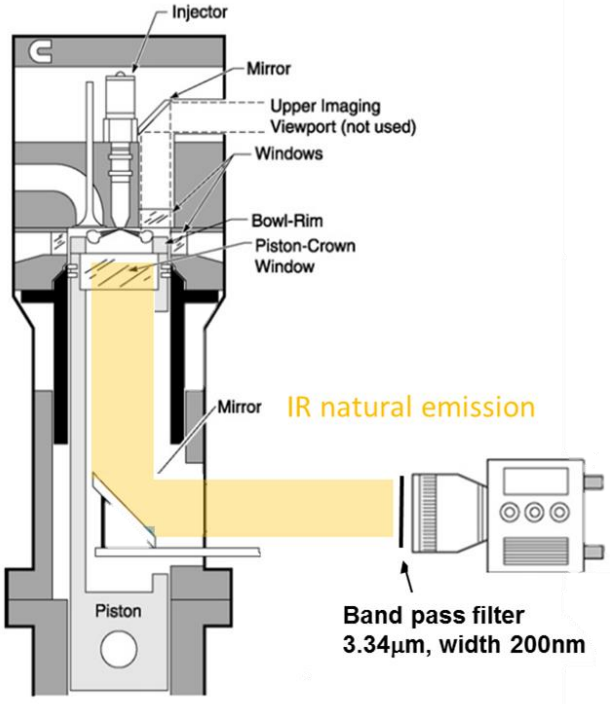

Figure 1: Extended-piston optical imaging schematic for IR detection.

only the temperature to affect the IR emission along the jet axis. Assuming adiabatic mixing, the temperature increases according to the heat capacities of the fuel and air, approaching an asymptote at the ambient gas temperature. The IR emission intensity of a non-reacting jet should display a similar behavior, increasing with downstream distance from the injector and asymptotically approaching a steady level far downstream. IR emission from reacting jets is expected to display a complicated behavior, where exothermic reactions increases the local temperature, but also consume the available C-H stretch-band emitters.

Collecting IR emission near 3.4 micron wavelength is favorable for hydrocarbon detection because it is relatively free of interference from CO, CO_2 and H_2O [5]. Nevertheless, depending on the filter passband, some other minor emissions may be present. H_2O emission with emissivity of up to 0.4 between 2.9 to 3.1 micron as predicted by the HITRAN spectral model may interfere with the vapor fuel emission under reacting conditions [5]. HCHO also has a weak emission line at 3.6 microns, and OH also emits very weakly (up to 0.01 emissivity) between 2.6 to 3.4 micron [5].

Each IR emission image is from a different engine cycle, captured from 2 degrees crank-angle (°CA) after the start of injection (ASI) to 10 ASI using a 5 microsecond exposure. Start of injection occurs at 355 crank-angle degrees (CAD) of the compression stroke (with TDC at 360 CAD). Referring to the AHRR for 'Spray B' [12], these image timings span both first- and second-stage ignition for the 1000 K and 900 K conditions, but only first-stage ignition is captured for the 800 K condition, with the transition to second-stage ignition beginning just after the end of the image sequence.

3. Results and Discussion

Instantaneous images of the non-reacting (top) and combusting jets (bottom) are presented at each TDC temperature at four selected timings in the cycle in Fig. 2. Reflections of IR emission off the different engine head materials lead to differences in the detected intensity. Reflections from the bowl wall near 50 mm are

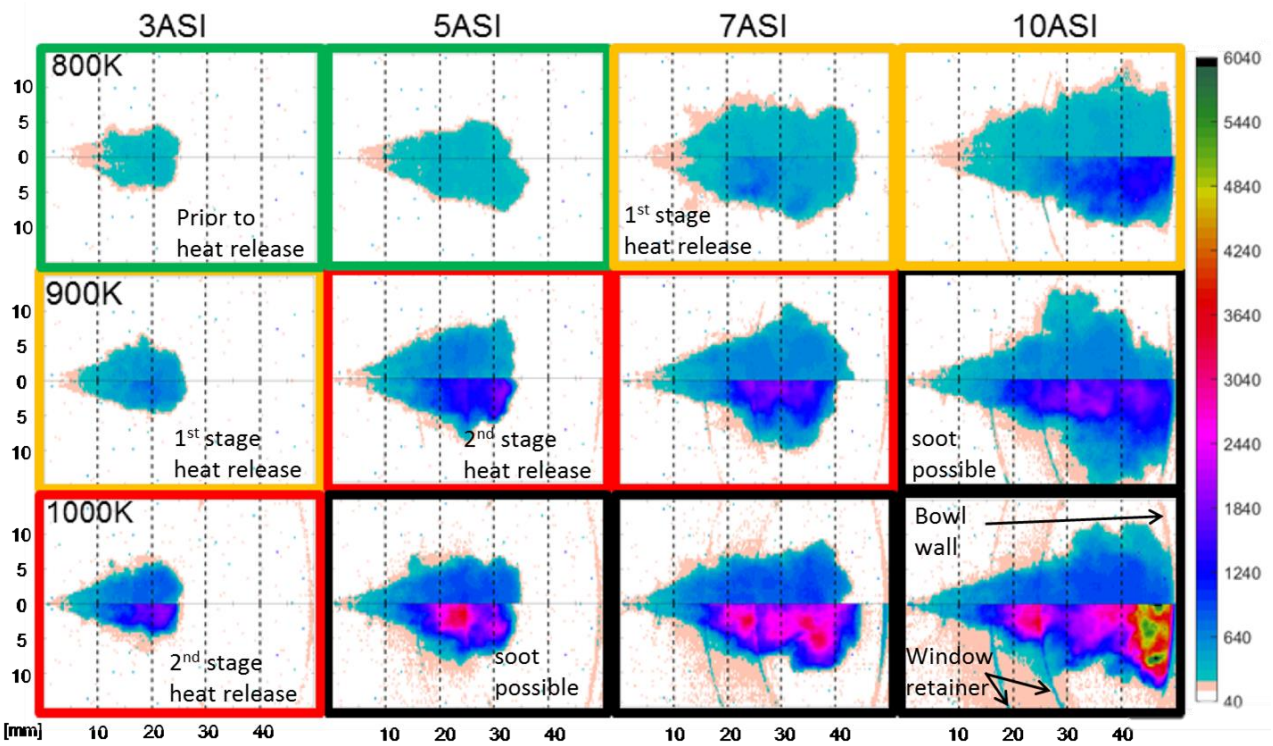

Figure 2: Instantaneous IR emission images at various ASI timings. Each image tile is a composite of non-reacting (top) and combusting (bottom) conditions. The injector is on the left side of the images, and the scale at the bottom indicates the distance from the injector. Color coding is added in the border of each tile to indicate stage of heat release, as determined from [12]. The same color scale in arbitrary units of pixel intensity is applied to all images.

also visible. Profiles of ensemble average data at 7 ASI for each temperature appear in Fig. 3. Important observations include:

- Consistent with jet penetration correlations and schlieren imaging [11], we see in Fig. 2 that under constant-density non-reacting conditions, variations in ambient-gas temperature do not noticeably affect penetration.
- Axially, the jet centerline intensity increases with downstream distance and reaches a plateau from 25 to 40 mm downstream, (Fig 3.) The emission increase between the injector tip to 25 mm downstream is consistent with expectations of an asymptotic trend and 1D model predictions [9], but the sudden plateau at the window interface is not expected based on jet emission considerations alone. Fluid dynamics associated with the jet head may create a different mixing/temperature distribution than the steady jet conditions measured in [17], and mixing measurements during transient conditions are not yet readily available.
- The slope change at the window interface strongly suggests that metal-surface reflections yield different signal distributions than window reflections and/or transmission effects are different.

This last point is based on earlier reasoning that, to first order, the IR intensity should depend on temperature alone. A plateau in intensity suggests that mixtures and therefore temperature in the jet head are relatively uniform. Indeed, previous laser-Rayleigh-scatter imaging of diesel jets show relatively uniform mixtures at the jet head [13]. Hence, the combination of a background material change and jet-head fluid dynamics that are different than the steady-jet assumptions of the models likely yield this unexpected axial intensity plateau, suggesting a balance between lower fuel-vapor concentrations and increasing entrainment downstream yielding relatively constant temperature.

The axial variation in longitudinally integrated emission is compared between the non- reacting and reacting cases at each temperature and is shown in Fig. 3. For the reacting conditions, the 2-fold increase in intensity with reaction is modest compared to the 10-fold increase that would be expected from the factor 2 to 3 increase in temperature due to combustion. This suggests that emission from hot products do not significantly contribute within the 3.2-3.5 micron passband, and that reductions in the number of C-H bonds due to reaction offset the signal increase due to temperature rise. Hence, even with combustion, the IR signal likely arises primarily from hot intermediate reaction species with C-H bonds 'inside' the jet during the

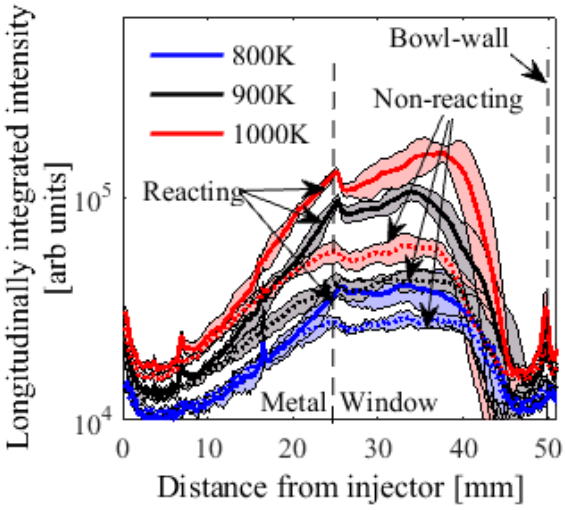

Figure 3: Ensemble-averaged longitudinally integrated emission profiles at 800, 900 and 1000K comparing non-reacting (dotted) and combusting (solid lines) conditions at 7 ASI. Shaded bands indicate 95% confidence interval on the mean of 30 processed images.

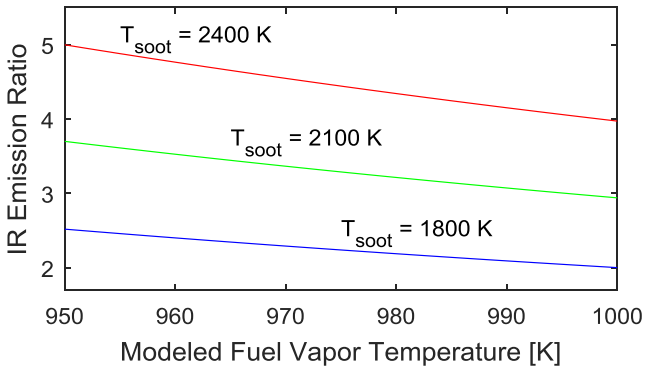

Figure 4: Ratio of modeled IR emission from soot relative to that from non-reacting fuel vapor, based on ECN 'Spray A' data [15,17], corresponding to a central location in the jet 45 mm downstream from the nozzle, at experimental conditions of 1000 K ambient gas temperature at 10 ASI.

combustion event, at least for the first few °CA following ignition, before a significant amount of soot is produced.

Several °CA after the onset of main ignition, for instance in the 1000K images in Fig. 2 at 10ASI, pockets of high intensity appear, especially near the bowl wall in the head of the jet. Compared to the non-reacting jet, there are local regions that show an increase in infrared signal by a factor of more than seven. This could be from broadband soot incandescence, or may be an increase in mixing of the hot combustion product gases due to impact with the bowl wall of the relatively rich mixtures in the core of the jet prior to their complete reaction.

To estimate the expected infrared emission contribution from soot, we compute the emissivity of soot as a function of previously measured soot volume fraction (10ppm) and path length (15mm) at approx. 45mm downstream under similar conditions from the Spray A database on the Engine Combustion Network [14-15], which yields an emissivity of 0.27 in the 3.2-3.5 micron filter passband. Similarly, for previously measured Spray A fuel-vapor mixture fraction (0.07) [17] and with the effective absorption cross section (43 m^2/mol) [16] yields an emissivity of 0.98. The soot and vapor-fuel temperatures have not been measured, but the ratio of emissive power for soot relative to vapor fuel is shown in Fig. 4 for a range of likely temperatures. These bounding calculations estimate soot emission to be two to five times higher than fuel alone, which is comparable to the factor of seven increase observed in the bright emission pockets.

4. Limitations, Uncertainties, and Future Work

Several improvements to the results are possible by addressing the following known issues. The change in absorption cross section with composition of the gases during reaction needs to be assessed. Also in the case of reaction, the jet will experience expansion and a widening of the jet angle. These physics are not present in the path-length approximations made here, but impacts are expected to be small since the widening is likely due to the expansion of products which are not expected to contribute significantly to the detected signal at these wavelengths. Emission and scattering from liquid-phase fuel have not been considered. The simple estimates for contributions from soot can be better elucidated through comparison with simultaneous soot extinction and IR emission data. Continued work with fuels and novel diagnostic techniques at ECN conditions help to build an ever growing database and continue to enable the type of uncertainty estimates provided here.

5. Conclusions

Infrared imaging of hydrocarbon C-H stretch band emission at 3.2-3.4 micron is compared at non-reacting and reacting conditions and appears to be a viable method to detect vapor fuel during direct-injection diesel combustion prior to soot formation. Comparisons of experimental IR-emission images of a non-reacting and a reacting jet are generally consistent with literature expectations for jet penetration.

- IR emission increases with downstream distance from the injector in both cases. (Figs. 2 and 3)
- In both cases, a plateau of nearly constant intensity in the head of the developing jet is consistent with relatively uniform mixtures previously measured in the heads of diesel jets. (Figs. 2 and 3)
- After ignition, prior to soot formation, IR emission increases only modestly, by a factor 1.5-2. (Fig. 3)
- When soot is likely present, e.g. after the end of the premixed burn, pockets of emission increase by a factor of more than 7 when compared to a non-reacting jet. (Fig. 2, e.g. 10ASI @1000K)
- A bounding analysis of estimated signals suggests that 50% to 80% of the emission increase could be attributed to broadband soot, when present. (Fig. 4)

The observations demonstrate the limits of IR imaging to track vapor fuel and provide new insight into mixture formation during combustion and in the presence of soot. More work is yet needed to better quantify contributions from emitter concentration, path length, species molar emissivity to the IR emission under combusting conditions. Given the above, we suspect that simultaneous high-speed soot

extinction and IR vapor fuel emission may be helpful to determine fate and transport of fuel vapor that becomes soot.

6. Acknowledgements

Experiments were conducted at the Combustion Research Facility, Sandia National Laboratories, Livermore, CA. Support for this research comes from the U.S. Department of Energy, Office of Vehicle Technologies. Sandia is a multi-mission laboratory operated by Sandia Corporation, a Lockheed Martin Company for the United States Department of Energy's National Nuclear Security Administration under contract DE-AC04-94AL85000. The authors thank Dave Cicone for his assistance maintaining the research engine. The significance of a consistent fuel and experimental conditions made available in the ECN database provided resources and support to our understanding. The availability of data and its utility as a baseline for reference comparisons, as well as the increased impact and scientific benefit of testing at ECN conditions is gratefully acknowledged.

7. References

[1] W. G. Agnew, J. T. Agnew, and K. Wark, *Infrared emission from cool flames Stabilized cool flames; Engine cool flame reactions; Gas temperatures deduced from infrared emission*, Proc. Combust. Inst. 5 (1955) 766–778.
[2] H. Jiang, Y. Qian, and K. T. Rhee, *High-speed dual-spectra infrared imaging*, Optical Engineering 32 (1993).
[3] L. S. Rothman, C. P. Rinsland, et al., *The HITRAN molecular spectroscopic database and hawks (HITRAN atmospheric workstation)*: 1996 Ed., J. Quant. Spectrosc. Radiat. Transfer 60 (1998) 665–710.
[4] A. E. Klingbeil, J. B. Jeffries, and R. K. Hanson, *Temperature-dependent mid-IR absorption spectra of gaseous hydrocarbons*, J. Quant. Spectrosc. Radiat. Transfer 107 (2007) 407–420. doi: 10.1016/j.jqsrt.2007.03.004.
[5] M. Jansons, S. Lin, and K. T. Rhee, *Infrared spectral analysis of engine preflame emission*, Int. J. Engine Res. 9 (2008) 215–237. doi: 10.1243/ 14680874JER00408.
[6] E. Mancaruso, L. Sequino, and B. M. Vaglieco, *IR digital imaging for analyzing in- cylinder combustion process in transparent diesel engine*, (2014) Fotonica AEIT Italian Conference on Photonics Technology.
[7] E. Mancaruso, B. M. Vaglieco, and L. Sequino, *Using 2d Infrared Imaging for the Analysis of Non-Conventional Fuels Combustion in a Diesel Engine.* SAE Int. J. Engines, 8(4) (2015) 1701-1715. https://doi.org/10.4271/2015-01-1646.
[8] C. W. Squibb, H. Schock, et al., *A demonstration of simultaneous infrared and visible imaging techniques with pressure data in an optically accessible diesel engine operating at part load with high EGR*, SAE Tech. Paper (2011) 2011–01–1395. doi: 10.4271/2011-01-1395.
[9] W. E. Eagle, L.-M. Malbec, and M. P. B. Musculus, *Comparing vapor penetration measurements from IR thermography of C-H stretch with schlieren during fuel injection in a heavy-duty diesel engine*, 9th US National Combustion Meeting (2015).
[10] M. P. B. Musculus, J. E. Dec, and D. R. Tree, *Effects of fuel parameters and diffusion flame lift-off on soot formation in a heavy-duty DI diesel engine*, SAE Technical Paper 2002-01-0889 (2002). https://dx.doi.org/10.4271/2002-01-0889.
[11] W. E. Eagle, L.-M. Malbec, and M. P. B. Musculus, *Measurements of liquid length, vapor penetration, ignition delay, and flame lift-off length for the Engine Combustion Network "Spray B" in a 2.34 L heavy-duty optical diesel engine*, SAE Int. J. Engines 9(2) (2016) 910-931. https://doi.org/10.4271/2016-01-0743
[12] E. Tomita, N. Kawahara, and A. Nishiyama, *In situ measurement of hydrocarbon fuel concentration near a spark plug in an engine cylinder using the 3.392 μm infrared laser absorption method: application to an actual engine*, Meas. Sci. Technol. 14 (2003) 1357–1363.
[13] C. Espey, J. Dec, T. Litzinger, and D. Santavicca, *Planar laser rayleigh scattering for quantitative vapor-fuel imaging in a diesel jet*, Combust. Flame 109(1–2) (1997) 65–86.
[14] M. Musculus, *Measurements of the influence of soot radiation on in-cylinder temperature and exhaust NOx in a heavy-duty DI diesel engine*, SAE Technical Paper 2005-01-0925 (2005). doi:10.4271/2005-01-0925.
[15] S. Skeen, J. Manin, K. Dalen, and L. Picket, *Extinction-based imaging of soot processes over a range of diesel operating conditions*, 8th US National Combustion Meeting (2013).
[16] A. Klingbeil, *Mid-IR laser absorption diagnostics for hydrocarbon vapor sensing in harsh environments*, Ph.D Thesis, Stanford University (2007).
[17] L. Pickett, J. Manin, C. Genzale, D. Siebers, M. Musculus, and C. Idicheria. *Relationship between diesel fuel spray vapor penetration/dispersion and local fuel mixture fraction,* SAE Int. J. Engines 4(1) (2011) 764-799. https://doi.org/10.4271/2011-01-0686